

**DEVELOPMENT OF AN AUTOMATIC  
CALCULATION METHOD FOR CT DOSE  
ESTIMATION BASED ON INDIVIDUAL  
SPECIFIC SIZE IN PAEDIATRIC POPULATION**

**MUHAMMAD KABIR ABDULKADIR**

**UNIVERSITI SAINS MALAYSIA**

**2022**

**DEVELOPMENT OF AN AUTOMATIC  
CALCULATION METHOD FOR CT DOSE  
ESTIMATION BASED ON INDIVIDUAL  
SPECIFIC SIZE IN PAEDIATRIC POPULATION**

by

**MUHAMMAD KABIR ABDULKADIR**

**Thesis submitted in fulfilment of the requirements  
for the degree of  
Doctor of Philosophy**

**May 2022**

## ACKNOWLEDGEMENT

I would like to express my gratitude to Allah SWT for giving me opportunity and help me endlessly in finishing the PhD research. I would like to express my deep and sincere gratitude to my supervisor, Dr. Noor Diyana Osman for giving me the opportunity to do the research and providing invaluable guidance and support throughout this research. Her dynamism, simplicity, sincerity and vision have immensely inspired me. A very special gratitude goes out to my co-supervisors, Prof., Ibrahim Lutfi Shuaib, Dr., Anusha Achutan and Dr. Radin Nasirudin for their guidance and contributions to this research.

I am grateful to my parents and in-laws for their love, prayer, sacrifices, care and support during this period. I am extremely grateful to my dear wife and children for understanding and persevering with me throughout this study. I would also like to acknowledge the Fundamental Research Grant Scheme (FRGS) (Project code: FRGS/1/2019/STG02/USM/02/6) by Ministry of Education (MOE), Malaysia for funding this research. I am equally grateful to the Tertiary Education Trust Fund, Nigeria for the sponsorship and support.

My sincere gratitude goes to all the staff of the Imaging unit, Advanced Medical and Dental Institute, USM for always being available to render assistance during data collection. I would also like to thank them for their friendship, hospitality and care.

## TABLE OF CONTENTS

<b>ACKNOWLEDGEMENT</b> .....	<b>ii</b>
<b>TABLE OF CONTENTS</b> .....	<b>iii</b>
<b>LIST OF TABLES</b> .....	<b>vi</b>
<b>LIST OF FIGURES</b> .....	<b>viii</b>
<b>LIST OF SYMBOLS</b> .....	<b>xii</b>
<b>LIST OF ABBREVIATIONS</b> .....	<b>xiii</b>
<b>LIST OF APPENDICES</b> .....	<b>xiv</b>
<b>ABSTRAK</b> .....	<b>xvi</b>
<b>ABSTRACT</b> .....	<b>xviii</b>
<b>CHAPTER 1 INTRODUCTION</b> .....	<b>1</b>
1.1 Background of the study .....	1
1.2 Problem statement and study rationale.....	3
1.3 Objective of the study .....	5
1.3.1 Specific Objectives.....	6
1.4 Significance of the study .....	6
1.5 Scope of the study .....	7
1.6 Thesis Organisation.....	7
<b>CHAPTER 2 LITERATURE REVIEW</b> .....	<b>9</b>
2.1 Computer Tomography (CT) scan .....	9
2.1.1 Principle of CT .....	10
2.1.2 CT generations .....	12
2.2 Computed Tomography Dosimetry.....	15
2.2.1 Dose Distribution in CT .....	16
2.2.2 CT-Specific Dose Quantities.....	18
2.2.3 Size-specific Dose Estimate (SSDE).....	22

2.2.4	Other dose quantities .....	25
2.2.5	CT Dosimetry Phantom.....	27
2.3	Dose Optimisation in Computed Tomography .....	28
2.3.1	CT Scanner Technology.....	29
2.3.2	Diagnostic Reference Levels (DRLs) and Dose Audit .....	33
2.3.3	Personnel Training .....	34
2.4	Algorithm .....	35
2.5	Radiation risk in paediatric CT .....	38
2.6	Patient radiation dose quantification in CT.....	43
2.7	Impact of patient size in CT dose estimation .....	45
2.8	Patient size determination for SSDE.....	50
2.9	Automated patient's size determination and SSDE calculation.....	52
2.10	SSDE and organ dose estimation .....	53
2.11	Diagnostic Reference Levels (DRL) in paediatric CT.....	55
	<b>CHAPTER 3 METHODOLOGY.....</b>	<b>58</b>
3.1	Research Tools .....	58
3.2	Study design .....	63
3.3	Research Methodology.....	68
3.3.1	Assessment of paediatric CT protocols and associated dose .....	68
3.3.2	Size estimation and size-specific dose estimation.....	71
	3.3.2(a) Determination of patient size (manual) .....	72
3.3.3	Development and validation of automated SSDE calculator.....	77
3.3.4	Evaluation of the discrepancy between CTDI <sub>vol</sub> and SSDE.....	86
	<b>CHAPTER 4 RESULTS AND DISCUSSION.....</b>	<b>87</b>
4.1	Retrospective survey on local paediatric CT scans .....	87
4.1.1	Patient demography.....	87
4.1.2	Paediatric CT protocol parameters.....	89

4.1.3	Local dose distribution (CTDI <sub>vol</sub> and DLP) .....	92
4.2	Size values and SSDE values for paediatric.....	101
4.2.1	Paediatric patient size (Manual calculation) .....	101
4.2.2	The reference values for paediatric SSDE .....	118
4.3	Automated patient size and SSDE calculator.....	123
4.4	SSDE and CTDI <sub>vol</sub> .....	133
4.4.1	Major Contribution.....	137
<b>CHAPTER 5 CONCLUSION.....</b>		<b>139</b>
5.1	Conclusion.....	139
5.2	Limitations of the study.....	141
5.3	Future works.....	142
<b>REFERENCES.....</b>		<b>143</b>
<b>APPENDICES</b>		
<b>LIST OF PUBLICATIONS</b>		
<b>LIST OF CONFERENCE PRESENTATIONS</b>		

## LIST OF TABLES

	<b>Page</b>
Table 2.1	The overview of CT generations..... 13
Table 3.1	Properties of CT scanners used in this study .....58
Table 3.2	The size conversion factors for $CTDI_{vol}$ to SSDE provided by AAPM (Boone et al., 2011) .....61
Table 4.1	Summary of acquisition parameters during paediatric CT examination.....89
Table 4.2	Comparison of local paediatric CT protocols with the optimised protocols for Siemens CT scanner (Nivelstein et al., 2010).....90
Table 4.3	Comparison of acquisition protocols for paediatric CT scanning.....92
Table 4.4	Summary of the distribution (range, mean, standard deviation) of paediatric head and abdomen sizes ( $D_{eff}/D_w$ )..... 101
Table 4.5	Size distribution in effective diameter, water equivalent diameter, anteroposterior, lateral axial and lateral topography dimensions of measured paediatric head ..... 102
Table 4.6	Size distribution in effective diameter, water equivalent diameter, anteroposterior, lateral axial and lateral topography dimensions of measured paediatric abdomen ..... 102
Table 4.7	Comparison of paediatric sizes from this study with values reported in other studies used for determination of maximum difference for head CT ..... 112
Table 4.8	Comparison of paediatric sizes from this study with values reported in other studies used for determination of maximum difference for abdomen CT ..... 112
Table 4.9	The comparison of paediatric size (anteroposterior diameter) from this study with values reported in other studies for abdomen..... 113

Table 4.10	The comparison of paediatric size (Axial, lateral diameter) from this study with values reported in other studies for abdomen.....	113
Table 4.11	The comparison of paediatric size (Topography, lateral diameter) from this study with values reported in other studies for abdomen.	114
Table 4.12	Shows the result of Pearson’s correlation of patients’ size with size dependent variables for Abdomen CT .....	115
Table 4.13	Shows the result of Pearson’s correlation of patients’ size with size dependent variables for head CT .....	115
Table 4.14	DRL, DRR and achievable dose distribution of SSDE for head and abdomen .....	120
Table 4.15	Comparison of SSDE derived from $D_{eff}$ and $D_w$ .....	121
Table 4.16	Comparison of SSDE-based DRL from this study and International DRLs .....	122
Table 4.17	Agreement between patient size measurement, derived from manual ( $D_{eff}$ ) and algorithm measurement.....	124
Table 4.18	Variability of Agreement between patient size measurement, derived from manual ( $D_{eff}$ ) and $D_w$ compared to Algorithm measurement .....	129
Table 4.19	Comparison of size determination error obtained from AAPM, (2014), Anam et al., (2016), Juszczuk et al., (2021) and this study. ....	132
Table 4.20	Difference between paediatric dose before and after size correction .....	134



## LIST OF FIGURES

	<b>Page</b>
Figure 2.1	Multiple projections of x-ray beam captured by the electronic detectors as the x-ray beam passes through the patient trunk while rotating around the patient. (From CT Scans, by America Physical Society, Copyright 2021 by America Physical Society)..... 11
Figure 2.2	Multi-slice with helical CT configuration. (From Multislice computed tomography by CADTH. Copyright 2014 by Canadian Agency for Drugs and Technologies in Health). ..... 15
Figure 2.3	Illustration of spatial dose distribution and isodose dose lines in projection radiography (a) and CT (b). From Computed Tomography by Buzug, 2008. Copyright by Springer Nature Switzerland AG..... 17
Figure 2.4	Illustration on single slice dose profile for (a) nominal slice thickness of 10mm and (b) computed tomography dose index (CTDI) obtained via the area of dose profile. ( Buzug, 2008). ..... 18
Figure 2.5	CTDI phantoms of 16 cm and 32 cm in diameter (polymethyl-Methacrylate). (From CT Dose Phantoms by Universal Medical. Copyright 1983-2021 by Universal Medical) ..... 19
Figure 2.6	Illustration of CTDI dose quantification. (From International Atomic Energy Agency (IAEA), L06 radiation protection in CT. Copyright 2009 by IAEA)..... 22
Figure 2.7	The CTDI PMMA body and head phantoms, with the holes (notches) representing the periphery and central measurement points. .... 28
Figure 2.8	Angular, longitudinal and combined tube current modulation from (Rego et al., 2007, Copyright 2007 by Mayo Clinic) ..... 30
Figure 2.9	Lifetime attributable cancer mortality risk as a function of age at a single acute exposure by National Academy of Sciences BEIR V

	(Biological Effects of Ionising Radiations) committee (solid line) and the ICRP (International Commission on Radiological Protection) report 60 (dotted line). (Brenner et al., 2001). ....	40
Figure 2.10	Estimated age-dependent CT doses to various organs that contribute significantly to overall estimated risk for typical single CT examination of head and of abdomen. (Brenner et al., 2001). ....	41
Figure 2.11	Risk per unit dose for common Cancer types in females and males. (Brenner et al., 2001). ....	42
Figure 2.12	Typical variation of patient body size with age .....	45
Figure 3.1	The Siemens SOMATOM Definition AS + CT at AMDI, USM with phantom setup and dosimeter positioned for dose measurement .....	59
Figure 3.2	The flow chart of the study .....	64
Figure 3.3	Flowchart describing the investigation of paediatric CT protocols and patient doses .....	69
Figure 3.4	The process for the calculation of SSDE .....	72
Figure 3.5	Illustration of measurement of AP and lateral dimension on axial abdomen and head CT images for determination of $D_{eff}$ .....	73
Figure 3.6	Illustration of measurement of water equivalent diameter ( $D_w$ ) on axial CT image .....	74
Figure 3.7	The flow chart of SSDE auto-calculator algorithm .....	78
Figure 3.8	Image Segmentation and thresholding process; (A) phantom, (B) thorax, (C) head and (D) abdomen.....	80
Figure 3.9	Plot of size correction factor ( $f$ ) against Patient size (effective diameter) in cm. ....	82
Figure 3.10	Operational flow chart of automated size and dose calculator (algorithm).....	83
Figure 4.1	Distribution of paediatric patients based on number of scan phase they underwent .....	88

Figure 4.2	Box-plot showing the median and interquartile range of estimated paediatric dose for each age group represented as (a) $CTDI_{vol}$ and (b) DLP for head CT scan and (c) $CTDI_{vol}$ and (d) DLP for abdomen CT scan. Data are defined as median (horizontal line inside boxes), interquartile range (boxes), and highest and lowest values (ends of whiskers).....	94
Figure 4.3	Comparison of age-based paediatric doses in (A) $CTDI_{vol}$ and (B) DLP from routine head CT examination of Malaysian and Nigerian studies.....	96
Figure 4.4	Comparison of 3 <sup>rd</sup> quartile dose values received from paediatric head CT scan; (A) $CTDI_{vol}$ (mGy) and (B) DLP (mGy.cm) of this study with other established DRLs. ....	98
Figure 4.5	Comparison of 3 <sup>rd</sup> quartile dose values received from paediatric abdomen CT scan (A) $CTDI_{vol}$ (mGy) and (B) DLP (mGy.cm) of this study with other established DRLs.....	99
Figure 4.6	The relationship and correlation between $D_{eff}$ and $D_w$ for (A) head and (B) abdomen in paediatric population.....	104
Figure 4.7	Scatter plot showing correlation of age with paediatric size ( $D_{eff}$ ). Plot (A) and (B) plots for head and abdomen respectively.....	106
Figure 4.8	Plot of $CTDI_{vol}$ -to-SSDE conversion factor (f) in relation to patient sizes ( $D_{eff}$ and $D_w$ ) and their coefficient of determination.....	109
Figure 4.9	The plots of the average body size [head (a) and abdomen (b)] from this study in comparison to other studies .....	111
Figure 4.10	Scatter plot showing the relationship between size ( $D_{eff}$ and $D_w$ ) and mAs, $CTDI_{vol}$ and SSDE .....	117
Figure 4.11	Box plot graphs (A& B) showing the distribution of SSDE according to age group.....	119
Figure 4.12	Bland-Altman plot of difference between manual $D_{eff}$ and automated algorithm on (A) patient images and (B) Phantoms.....	125

Figure 4.13	Combined Correlation of results of manual ( $D_{\text{eff}}$ and $D_w$ ) and automated measurement.....	127
Figure 4.14	Bland-Altman plot of difference between patient size measurement, derived from manual ( $D_w$ ) compared to Algorithm measurement .....	129
Figure 4.15	Bland-Altman plot of difference between patient size measurement, derived from manual ( $D_{\text{eff}}$ ) and ( $D_w$ ) compared to Algorithm measurement.....	131
Figure 4.16	Discrepancies between dose before ( $\text{CTDI}_{\text{vol}}$ ) and after (SSDE) size correction in (A) head and (B) abdomen CT examinations.....	137

## LIST OF SYMBOLS

Gy	Gray
$D_w$	Water equivalent diameter
$D_{\text{eff}}$	Effective diameter
wT	Tissue weighting factor
wr	Radiation weighting factor
$D(z)$	Radiation dose along Z-axis
d	Nominal slice thickness
N	Number of tomographic sections
T	Width of the tomographic section along z-axis or nominal scan width
l	Table increment per gantry rotation
A	Area
$\pi$	Ratio of a circle's circumference to its diameter, approximately equals 3.1414
B16	Denotes the use of 16 cm phantom size for body $CTDI_{\text{vol}}$
B32	Denotes the use of 32 cm phantom size for body $CTDI_{\text{vol}}$
H16	Denotes the use of 16 cm phantom size for head $CTDI_{\text{vol}}$
$\sigma$	Standard deviation
Z	Level of significance
E	Accuracy of estimate or margin of error
%	Percentage

## LIST OF ABBREVIATIONS

AAPM	American Association of Physicist in Medicine
ACR	American College of Radiology
AP	Anterior posterior
BMU	Best Matching Unit
CT	Computed Tomography
CTDI	Computed Tomography Dose Index
CTDI <sub>vol</sub>	Volume weighted Computed Tomography Dose Index
DLP	Dose Length Product
DRL	Diagnostic Reference Level
DRR	Diagnostic Reference Range
D <sub>eff</sub>	Effective Diameter
D <sub>w</sub>	Water equivalent Diameter
E	Effective Dose
F	CTDI <sub>vol</sub> -to-SSDE Conversion Factor
DICOM	Digital Imaging and Communications in Medicine
mGy	Milli Gray
CWM	Class Weight Matrix
CI	Confidence Interval
ICRP	International Commission for Radiation Protection
IAEA	International Atomic Energy Commission
LAT	Lateral
MATLAB	Matrix Laboratory
MSCT	Multislice Computed Tomography
PACS	Picture Archival and Communication System
SSDE	Size-specific Dose Estimate
USM	Universiti Sains Malaysia
PMMA	PolymethylMethacrylate
YR	Year

## LIST OF APPENDICES

Appendix A	Copy of study ethical approval I
Appendix B	Copy of study ethical approval II
Appendix C	Sample data for paediatric CT head protocol/dose
Appendix D	Sample data and statistical analysis for head protocol/dose
Appendix E	Protocol/dose data and statistical analysis for age group 1 (0-3 years) head CT
Appendix F	Protocol/dose data and statistical analysis for age group 2 (4-6 years) head CT
Appendix G	Protocol/dose data and statistical analysis for age group 3 (7-9 years) head CT
Appendix H	Protocol/dose data and statistical analysis for age group 4 (10-12) years head CT
Appendix I	Sample data for paediatric CT Abdomen protocol/dose
Appendix J	Sample data and statistical analysis for head protocol/dose
Appendix K	Protocol/dose data and statistical analysis for age group 1 (0-3 years) abdomen CT
Appendix L	Protocol/dose data and statistical analysis for age group 2 (4-6 years) abdomen CT
Appendix M	Protocol/dose data and statistical analysis for age group 3 (7-9 years) abdomen CT
Appendix N	Protocol/dose data and statistical analysis for age group 4 (10-12 years) abdomen CT
Appendix O	Sample SSDE data and statistical analysis for group 1 (< 1 year), head CT
Appendix P	Sample SSDE data and statistical analysis for group 2 (1-5 year), head CT
Appendix Q	Sample SSDE data and statistical analysis for group 3 (6-10 years), head CT
Appendix R	Sample SSDE data and statistical analysis for group 4 (10-12 years), head CT
Appendix S	Sample SSDE data and statistical analysis for group 1 (< 1 year), abdomen CT
Appendix T	Sample SSDE data and statistical analysis for group 2 (1-5 year), abdomen CT
Appendix U	Sample SSDE data and statistical analysis for group 3 (6-10 years), abdomen CT
Appendix V	Sample SSDE data and statistical analysis for group 4 (10-12 years), abdomen CT
Appendix W	Sample data for manual and automated measurement and calculations for head and thorax CT

Appendix X	Sample data for manual and automated measurement and calculations for abdomen CT
Appendix Y	Algorithm and code for the automated calculator
Appendix Z	Result of manual and automated measurement on phantoms



**PEMBANGUNAN KAEDAH PENGIRAAN AUTOMATIK UNTUK  
ANGGARAN DOS CT BERDASARKAN SAIZ SPESIFIK DALAM  
POPULASI PEDIATRIK**

**ABSTRAK**

Kaedah semasa bagi anggaran dos berdasarkan  $CTDI_{vol}$  dalam kalangan kanak-kanak menjurus kepada ketidaktepatan yang ketara dalam penganggaran dos kerana tidak mengambilkira saiz individu. Penganggaran dos berdasarkan spesifikasi saiz (SSDE) digunakan untuk pembetulan bagi kesan daripada penggunaan protokol CT semasa dan untuk mengurangkan dos dedahan radiasi kepada kanak-kanak yang diberikan lebih dua kali ganda daripada dos sepatutnya. Kajian ini bertujuan untuk menilai protokol CT semasa bagi kanak-kanak dan meminimumkan dos yang diterima oleh kanak-kanak semasa pemeriksaan pengimejan CT. Kajian ini juga bertujuan untuk membangunkan kaedah pengiraan automatik menggunakan algoritma MATLAB untuk pengiraan saiz pesakit dan SSDE yang lebih tepat. Tinjauan retrospektif dijalankan untuk menyiasat protokol pengimejan, dos berkaitan ( $CTDI_{vol}$ ), saiz pesakit (diukur secara manual  $D_{eff}$  dan  $D_w$ ) dan penganggaran SSDE untuk pesakit kanak-kanak yang menjalani pemeriksaan pengimejan CT kepala dan badan. Algoritma pengiraan automatik dibina menggunakan perisian MATLAB untuk pengukuran saiz pesakit ( $D_{eff}$ ) dan juga pengiraan SSDE. Data berangka yang dianalisis adalah parameter dedahan, anggaran dos ( $CTDI_{vol}$  dan SSDE), anggaran manual dan juga automatik bagi saiz pesakit,  $D_{eff}$ . Parameter dedahan dan dos ( $CTDI_{vol}$ ) dibandingkan dengan aras rujukan diagnostik (DRLs) sementara pengira automatik SSDE disahkan dengan pengukuran manual saiz dan pengiraan SSDE. Julat

rujukan diagnostik setempat dan taburan saiz pesakit diperoleh. Keputusan menunjukkan terdapat perbezaan 7 hingga 51% di antara  $CTDI_{vol}$  dan SSDE. Pengira automatik menghasilkan pengukuran saiz dan juga pengiraan SSDE yang lebih tepat dengan anggaran kesilapan kurang daripada 2%. Kesilapan pengukuran berdasarkan kaedah  $D_{eff}$  ini adalah lebih rendah dibandingkan dengan kajian lain dan di bawah daripada toleransi yang dibenarkan iaitu 10% dibandingkan dengan kaedah berdasarkan  $D_w$ . Sebagai rumusan, pengukur automatik yang dibangunkan berupaya mengukur saiz pesakit dan SSDE dengan tepat. Pengoptimuman protokol dedahan semasa penting bagi mengurangkan dos tempatan bagi pesakit kanak-kanak ( $CTDI_{vol}$ ).

**DEVELOPMENT OF AN AUTOMATED CALCULATION METHOD  
FOR CT DOSE ESTIMATION BASED ON INDIVIDUAL SPECIFIC SIZE IN  
PAEDIATRIC POPULATION**

**ABSTRACT**

The current dose estimation based on  $CTDI_{vol}$  in paediatric CT leads to significant inaccuracies in dose estimation due to inadequate size consideration. Size-specific dose estimate (SSDE) was employed to correct the effect resulting from the use of current CT protocols and minimise the radiation dose that been delivered more than double the intended dose to paediatric. This study aims to evaluate the current paediatric CT protocols and associated dose received by paediatric from CT scans. This study also aims to develop an automatic calculator using MATLAB algorithm for accurate patient size measurement and SSDE calculation. A retrospective survey was conducted to investigate CT protocols and associated dose ( $CTDI_{vol}$ ), patient size (manual measured  $D_{eff}$  and  $D_w$ ) and SSDE of paediatric patients undergoing head and abdomen CT scans. An automated calculation algorithm was developed on MATLAB platform for patient size measurement ( $D_{eff}$ ) and SSDE calculation. Numerical data analysed were scan parameters, estimated doses ( $CTDI_{vol}$  and SSDE), manual and automated  $D_{eff}$  estimates of patient size. Scan parameters and dose ( $CTDI_{vol}$ ) were compared with diagnostic reference ranges (DRLs) while automated SSDE calculator was validated with the manual size measurement and SSDE calculation. Local diagnostic reference ranges and patient size distribution were derived. The results showed a disparity of 7 to 51% between  $CTDI_{vol}$  and SSDE. Automated calculator yields accurate measured size and calculated SSDE with an estimation error of less than 2%. The measurement error from the proposed  $D_{eff}$ -based method was lower

compared to other studies and below the acceptable tolerance of 10% compared to  $D_w$ -based method. In conclusion, the developed automated calculator is accurately and reliably measuring patient size and calculates SSDE. The optimisation of current CT protocols is important to minimise associated local paediatric dose ( $CTDI_{vol}$ ).

# CHAPTER 1

## INTRODUCTION

### 1.1 Background of the study

The use of computed tomography (CT) has increased significantly in the last decade for both paediatric and adult imaging (Bernier et al., 2019; Mettler et al., 2000). CT became the preferred imaging of choice as it has been proven to offer advantages in diagnostic capability and application in the detection of diseases as compared to other conventional diagnostic imaging modalities (Anam et al., 2016). However, CT is the highest contributor to global medical radiation (Mettler et al., 2000). The consistent annual global rise in the number of CT scans utilisation has become of concern because of the potential deleterious radiation effects especially in cancer induction. Therefore, accurate estimation of patient doses from CT exposures has become imperative, but the most challenging issues is to accurately determine dose to paediatric undergoing CT imaging.

CT dose data displayed as weighted computed tomography dose index ( $CTDI_w$ ), volume-weighted computed tomography dose index ( $CTDI_{vol}$ ) and dose length product (DLP). These dose descriptors are the bases of radiation dose quantification in CT dosimetry (International Electrotechnical Commission, 2002), that are referenced to measurement made on 16 and 32 cm polymethyl methacrylate (PMMA) phantoms (AAPM Task Group 111, 2010; Boone et al., 2011). However, these dose indices are described based on scanner output only and insufficient in considering the individual patient characteristics that determine attenuation such as size and homogeneity (McCollough et al., 2011). Consequently, previous study has found it to systematically trigger dose underestimation in paediatric and smaller adults

(Brady and Kaufman, 2012; Hossain, 2015; Huzail et al., 2018; J. Wang et al., 2012). Furthermore, the current CTDI method introduces a systemic error that limits the scanner's ability to make a distinction between two different patient sizes at a fixed scanner output setting.

Thus, it led to the introduction of the size-specific dose estimate (SSDE), which considers individual patient size in addition to scanner information by the American Association of Physicist in Medicine (AAPM). This method allows measured patient diameters with corresponding correction factors to be used to adjust or normalize the CT dose data ( $CTDI_{vol}$ ) to individual size. However, this approach looks simple in principle but very tedious in practice, especially the measurement of patient diameters from CT images, hence limiting the clinical adoption of the SSDE method. Automated methods for calculation and SSDE report was indicated as the major setback for the clinical implementation of SSDE (Boone et al., 2019).

Thus, accumulating accurate data of paediatric diameter ranges (patient size) became vital to contemporary dose estimation in CT, as well as the evaluation of the  $CTDI_{vol}$  application which ignores patient heterogeneity and size. Besides, the paediatric demography is critical compared to adults and therefore, they are more prone to the effects of radiation (Franck et al., 2018) and hence requires more attention for dose optimisation. Therefore, additional effort is required to refine existing paediatric CT dosimetry methods for more accurate means of determining radiation dose received from CT examinations.

Therefore, the careful consideration and deployment of algorithms for clinical evaluation have continue to increase as it offers reduced workload and improved task accuracy with less error (Cheng, 2013; Juszczyk et al., 2021; Regino et al., 2018).

Therefore, the purpose of this study was to evaluate paediatric CT protocols and associated dose received by paediatric undergoing CT scans and develop an automatic calculator using MATLAB algorithm for accurate paediatric size measurement and SSDE as described in AAPM report 204.

## **1.2 Problem statement and study rationale**

Theoretically, the radiation dose in CT imaging is dependent upon the CT scanner factors and patient characteristics. The scanner factor is inherent scanner design, technology and applied CT protocols and parameters (exposure factors). Patient factors constitute of patient size, body heterogeneity, and composition which determines x-ray attenuation. In current CT dosimetry, the  $CTDI_w$  or  $CTDI_{vol}$  is the basis of dose description to represent patient dose. However, the constraint of  $CTDI_{vol}$  and DLP is that they are proxies for patient dose rather than actual absorbed dose (Boone et al., 2011), as they did not take into consideration individual patient size and attenuation that substantially determine accurate absorbed dose. But instead, they only represent estimated dose based on phantom measurements of specific sizes and conditions.

The  $CTDI_w$  or  $CTDI_{vol}$  measurement and estimates are referenced to standard phantom sizes of 16 cm and 32 cm. Adult head and all types of paediatric scans are referenced to 16 cm and adult body to 32 cm sized phantom. The fact is, patient diameter varies and this variation is, more pronounce in paediatric population, as their sizes vary significantly with age as they grow (Boone et al., 2019; Strauss et al., 2013). Moreover, at present, the default CT protocols for paediatric body are not uniform, some manufacturers use the reference phantom size of 16 cm and others use the 32 cm for estimating  $CTDI_{vol}$  and DLP (Boone et al., 2011). Hence, paediatric doses may

not be accurately portrayed by the CT scanner due to apparent systemic error as a result of inadequate children size consideration inherent in current reference dosimetry calibration set-up. Furthermore, interpreting doses for the individual patient and comparison of paediatric dose becomes difficult.

Similarly, in the current clinical setting, inadequate children size consideration was demonstrated when a similar technique factor (radiation output) selected to scan two different patients of different sizes, results in the display of the same  $CTDI_{vol}$  value by the CT scanner. In this setting, smaller adults and paediatric may receive higher doses than large patients at the same radiation output. This implies that existing CT protocols delivers more than double the intended dose to children (Strauss et al., 2020). Similarly, existing pieces of literature corroborated this point with a report of up to about 50% underestimation of dose in children compared to adults as a result of the present setting and hence an inaccurate impression of radiation dose to the paediatric demography (Brady and Kaufman, 2012; Brink and Morin, 2012; Khawaja et al., 2015; Strauss et al., 2017). To address this problem, the SSDE was introduced. Thus, accumulating accurate information about patient size become critical for accurate individual patient dose assessment in CT imaging. Currently, there are no published reference ranges for paediatric diameter sizes for the Malaysian population that will guide clinicians in customizing patient CT dose or adopt SSDE.

Moreover, paediatric are the high risk-group and susceptible to the adverse effect of ionizing radiation because they are more radio-sensitive with rapidly dividing cells compared to adults with matured cells (Miglioretti et al., 2013). Besides, children have more years to live for the manifestation of the long-term radiation-related health effects and cancer induction (Bernier et al., 2019).



Furthermore, the SSDE approach is implied to correct the clinical deficiencies of the current  $CTDI_{vol}$  method by considering patient dimension in CT dose estimation. However, clinical measurements of patient diameter for SSDE are currently based on a manual approach that may be inconvenient, time-consuming and susceptible to inter-observer variability which may likely affect the accuracy of the patient size measurement (Khawaja et al., 2015; O'Neill et al., 2018). Manual measurement of patient size can also be time-consuming and tedious for the clinician, consequently, limiting the clinical implementation and adoption of the SSDE approach.

More so, the AAPM declared that the clinical adoption of the SSDE remains dependent on manufacturer implementation of methods to calculate and report SSDE (Boone et al., 2019) automatically. However, manufacturer automatic calculators are currently unavailable, hence, the need for the development of an automated dose calculator that will make SSDE easier and user-friendly for the clinician thereby increasing its clinical adoption and implementation for more accurate paediatric dose representation.

The purpose of this study was to evaluate paediatric CT protocols, dose (before and after size-correction), determine sizes of paediatric patients for SSDE and develop using MATLAB an algorithm for patient size measurement and SSDE dose calculator in line with the AAPM SSDE approach.

### **1.3 Objective of the study**

This study aimed to develop an automatic calculator for patient size measurement and size-specific dose estimation (SSDE).

### **1.3.1 Specific Objectives**

1. To assess the current scanning parameters and resulting dose distribution ( $CTDI_{vol}$ ) for paediatric undergoing head and abdomen CT scans.
2. To investigate the derived size-specific dose estimates (SSDE) for paediatric CT of the head and abdomen based on manually measured size.
3. To develop a validated algorithm-based automated calculator for patient size measurement and SSD estimation.
4. To determine the discrepancy between displayed dose ( $CTDI_{vol}$ ) and corrected dose based on SSDE in paediatric.

### **1.4 Significance of the study**

The result of this study will offer significant benefit to the clinician, CT practitioners, CT equipment manufacturers and paediatric patients undergoing CT imaging. The proposed automated calculator serves as a promising tool for the determination of the patient's diameter and dose estimation. The proposed algorithm offers a simple and user-friendly tool that requires less efforts, and time-consuming thereby influencing the clinical adoption for paediatric dose estimation based on specific individual size.

This study will enhance the current understanding of paediatric CT dosimetry. The outcome of this study will provide more insight into the accuracy, shortfalls, and elucidates alternative and more accurate approaches for dose description and determination in children. Diagnostic reference ranges (DRR) estimated in SSDE and diameter ranges will be beneficial to the clinician and health professional in ensuring optimisation of imaging practice and improvement of patient safety. Thus, it can also

contribute to a more extensive national reference database for quality assurance and dose audit.

The study may guide the manufacturer's choice of dose reference phantom and necessary amendments that may render CT machine output more appropriate for paediatric imaging. It may guide scanner manufacturers in the necessary adjustment of CT protocols to better suit this demography (paediatric) while eliminating the errors of dose underestimation among paediatric in existing CT scanners.

The safety and protection of children undergoing CT imaging will be enhanced as dose estimation using SSDE will account additional individual body size variation of the paediatric population into the current CT dosimetry practice. Furthermore, accurate dose to the patient can be determined while enhancing the monitoring and evaluation of potential risk associated with CT imaging.

## **1.5 Scope of the study**

This study evaluated children patients aged 0 to 12 years' old who underwent computed tomography scans of the head abdomen and chest at the Hospital Universiti Sains Malaysia (Kelantan, north-east of peninsula Malaysia), Advanced Medical and Dental Institute Universiti Sains Malaysia (Penang, north-west of peninsula Malaysia) and Usmanu-Dan Fodio University Teaching hospital, Nigeria between January, 2012 to February, 2021.

## **1.6 Thesis Organisation**

This thesis is organized into five distinct chapters. The first part of the chapter 1 is background; basic principles, brief history and application of CT dosimetry are outlined in order to define specific aspects of size-specific dose estimate in paediatric addressed in this study. An overview of the current dosimetry method and the

potentials of the newer SSDE method is highlighted. The chapter also outline the specific aims, scope and significance of this study. Chapter two extract potential evidence based methods and outcomes of the implementation of the old CT dose method in comparison to the newer size-based method. The basic physics and operational principles of CT and how they influence CT doses are discussed. Potential strategies for optimizing paediatric CT dose were also highlighted. Chapter 3 explains the research methods and various steps and settings that make up the study research method, sampling, techniques, instrumentation, test and statistical analysis used to achieve the set aims of this study. Chapter 4 highlights results and data generated from this study and discussed the research findings and its significance. Chapter 5 summarises the entire study, main findings and arguments to clarify the thesis. The chapter also highlights recommendations and limitations of the study.

## **CHAPTER 2**

### **LITERATURE REVIEW**

#### Preamble

This chapter presents a background, historical preview and relevant literatures about computed tomography. The section discusses the evolution, physics, technology and principles of CT scan and dose. This chapter aimed to explain the benefit of size-specific dose estimate in paediatric CT over existing CT dose metric based on evidence from literatures. Thus, it explains the need and justification for this study. It also highlights the relevance of automation and algorithm usage in medicine. It also highlights the conflicts and agreement of opinion from various stakeholders that revolves around SSDE implementation. Similarly, it explains the various approaches that informed and shaped the methodology adopted in this study.

#### **2.1 Computer Tomography (CT) scan**

Computed tomography (CT) is an imaging modality that utilises the principle of x-ray absorption and transmission to produce cross-sectional images with the aid of a computer system. The word "Tomos" is a Greek word meaning slice or section, while "Graphy" means study. The ability of CT to produce slice or sectional image clinically implies the possibility of imaging the body in more than two dimensions and hence more information about the object is available to the clinician for clinical decision making. CT was invented to supplement the conventional x-ray system, which produces two-dimensional images only (Bushberg et al., 2003).

The CT was developed based on a mathematical method of calculating radiation absorption distribution in the human body based on transmission measurement termed reconstructive tomography. Reconstructive tomography was first

successfully implemented into practice in 1972 by G. N. Hounsfield. Thus, it led to the invention of the CT scanner and subsequently, the production of the first clinical CT images of the human head (Kalender et al., 2008). The image proved convincing by detecting a cystic frontal lobe tumour and thus revolutionising radiology imaging and diagnosis. As a result, 60 CT scanners were installed as in 1974 and over 10,000 scanners in use as of 1980. Today CT scan accounts for more than 11% of medical procedures and contributes close to 50% of patient radiation doses from medical exposures (Al Mahrooqi et al., 2015). The continuous rise in CT usage was due to its increasing imaging and diagnostic capabilities as a result of steady advancement in CT technology especially the introduction of spiral CT (1989) and multi-slice (MSCT) capability that allows total body scans in few seconds as well as the availability of improved and robust image reconstruction algorithms. The number of clinical CT installations in 2010 was estimated to be above 50,000 and still on the rise. However, current global distribution of CT scanners is estimated in per one million of a population. In 2019, Japan had the highest of about 111.49 CT scanners per one million (“Computer tomography scanners density by country 2019 | Statista,” n.d.).

The invention of the CT scanner led to the award of the 1979 Nobel prize for Medicine to the duo of Godfrey Hounsfield and Allan Cormack (Kalender et al., 2008). The scanner is used for numerous diagnoses of human and animal diseases, treatment planning in radiotherapy, multi-modality diagnosis as in SPECT, PET/CT as well as in industrial applications, such as non-destructive testing and soil core analysis.

### **2.1.1 Principle of CT**

CT utilises x-rays together with an array of electronic detectors to record a pattern of densities arising from the object to create a slice image of the object or tissue.

The internal structure of objects is reconstructed from a series of projections of the object. The scanner assembly comprises of an x-ray beam from an x-ray tube rotating around the object within the scanner such that multiple x-ray projections are made across the object (Caldemeyer and Buckwalter, 1999). When x-rays transverse through the patient's body, the beam is attenuated. The degree of attenuation depends on the type of tissue through which the beam transverses. Image contrast in x-ray imaging is a result of the difference in attenuation between adjacent tissues. On CT, the higher the tissue attenuation of the x-ray beam, the brighter the tissue on CT image (bone, calcification) and the lower the attenuation, the darker the tissue appears on the CT image (fat, water, and air). Figure 2.1 depicts slice image acquisition at a collimated slice width in a multiple detector rows CT. The total beam width in the z-direction is set by pre-patient collimation and signals from every two or more detectors along the z-axis is electronically combined to form thicker slices (Flohr, 2013). This system offers a range of simultaneous acquisition thereby allowing shorter acquisition time and retrospective creation of thinner or thicker slices.

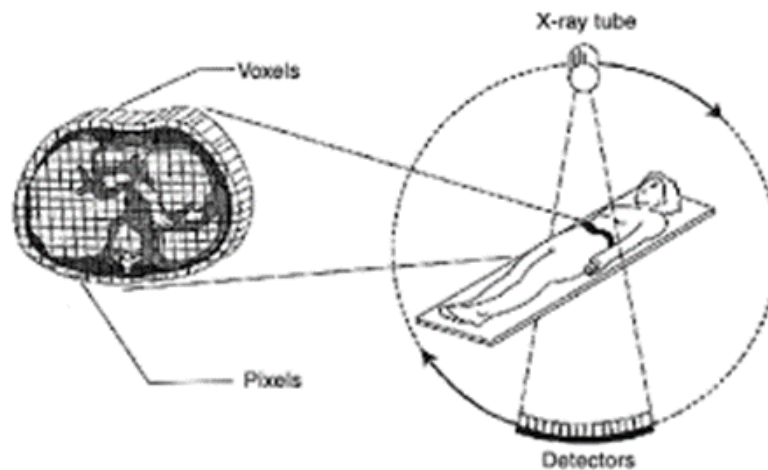


Figure 2.1 Multiple projections of x-ray beam captured by the electronic detectors as the x-ray beam passes through the patient trunk while rotating around the patient. From CT Scans, by America Physical Society, Copyright 2021 by America Physical Society

### 2.1.2 CT generations

CT technology has evolved and improved overtime. CT generations is a terminology used to describe the stages of technological progression of CT scanners. Currently, there are 6 generations of CT scanners (Generations 1-6). The geometrical designs of that distinguishes the various CT scanner generations are depicted in Table 2.1. The first generation is the earliest CT scanner having a parallel collimated pencil beam that uses a translate-rotate movement to cover the object. They were short lived because of long scan time of about 5 minutes to complete a single scan of a 180 ° degrees' rotation.

The earliest CT scanners operate on the stop and shoot mechanism or single slice CT (SSCT), as such required long acquisition time approximately 4.5 minutes of scan time to complete a brain scan (Brink et al., 1994). Thus, due to the long acquisition time of the scanner, there are concerns that CT scan of the thorax and abdomen might be impossible due to image degradation in the form of motion artefacts from organ movements such as heart and respiratory motion in this body region.

The second generation CT scanner have wider fan beam but with translate-rotate movement as in first generation. But fewer translate movement were required to acquire each view data. Besides, scan time is reduced by twenty seconds to two minutes. The third generation CT incorporates a fan beam geometry with the x-ray source and detectors (in arc arrangement) rotate together and it is known as rotate-rotate movement, thus allowing complete coverage of object at one time and a faster scanning time of about one seconds. Fourth generation scanner operates in a rotate-stationary movement with the x-ray source rotating around a ring of stationary detectors. This technology eliminates a large proportion of motion of scanner components associated with earlier generations and is enhanced with the slip ring



technology which allows transfer of electrical signal and power between a rotating machine and the external components.

Table 2.1 The overview of CT generations

<b>Generations</b>	<b>Source</b>	<b>Source Collimation</b>	<b>Detector</b>	
1 <sup>st</sup>	Single Tube	X-ray	Pencil Beam	Single
2 <sup>nd</sup>	Single Tube	X-ray	Fan Beam (not enough to cover FOV)	Multiple
3 <sup>rd</sup>	Single Tube	X-ray	Fan Beam (enough to cover FOV)	Curvilinear Array (x-ray source and detector moves)
4 <sup>th</sup>	Single Tube	X-ray	Fan beam covers FOV	Stationary Ring of Detectors
5 <sup>th</sup>	Many tungsten anode in single large tube		Fan Beam	Stationary Ring of Detectors
6 <sup>th</sup>	Single Tube	X-ray	Fan beam covers FOV	Curvilinear array (Table with patient moves)
7 <sup>th</sup>	Single Tube	X-ray	Cone Beam	Multiple array of detectors

The most significant innovation is the introduction of the slip-ring technology in 1989 that paved the way for spiral CT allowing simultaneous patient translation and x-ray exposure (Macari and Israel, 2002). Spiral CT enables a greater z-axis distance to be covered within a shorter time. Spiral CT allows multi-slice acquisition with multi-detector configuration incorporated in CT scanners. Though this advancement came with a disadvantage of increased volumetric data requiring processing units with high speed capacity, large memory and storage devices (Katada, 2002). However, the

technology proffers numerous possibilities and expanded the diagnostic capabilities of the modern CT scanner. It reduces artefact related to patient motion (voluntary and involuntary motions) and allows examination of specific areas at peak contrast uptake (Brink et al., 1994).

The basic idea of multi-slice computed tomography (MSCT) was to widen the imaging range in the z-direction with multiple rows of detectors (Figure 2.2). Thus data can be collected for multiple slices per scan (Goldman, 2008). This approach reduces the heat generated in the x-ray tube by reducing the number of tube rotations and therefore, the total usage of the x-ray tube needed to cover the desired anatomy. As the scan time is drastically reduced and whole-body scan is possible, and specialised examinations such as cardiac scans and dual-energy CT were possible. Today, the worldwide rising request for CT imaging is attributed to increasing diagnostic capability driven by the MSCT technology.

The size and quality of detectors affects spatial resolution of CT. The smaller detector size used in MSCT is usually compensated by a need of much higher tube currents to compensate the increase in image noise (Nieman et al., 2015). Nevertheless, MSCT offers spatial resolution of clinical benefit which offset the need for increased tube current utilisation (Nieman et al., 2015). Spatial resolution of an imaging system describes the system's ability to depict microstructures (Athanasίου et al., 2017).

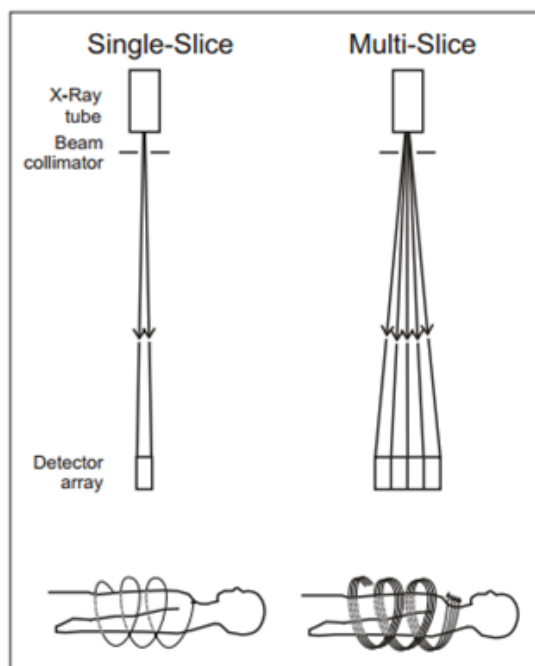


Figure 2.2 Multi-slice with helical CT configuration. From Multislice computed tomography by CADTH. Copyright 2014 by Canadian Agency for Drugs and Technologies in Health.

The fifth generation CT scanner technology eliminates all physical motion of source and detector components (stationary-stationary system) and is known as the electron beam CT (EBCT). The geometry in this technology is such that an electron beam is swept over a wide target to cover up to a half scan. This allows faster scanning and coverage and hence overcomes motion from patient organs as a complete scan can be achieved in about fifty milliseconds. This technology is widely used in cardiac imaging as its major advantage is the reduction of patient motion due to movement of the cardiac with short scanning time.

## 2.2 Computed Tomography Dosimetry

Radiation exposure conditions unique to CT imaging exist because the process of patient irradiation occurs with a narrow, fan-shaped x-ray beam delivered during x-ray tube rotation around the patient body. Thus, it required the use of dedicated

dosimetry techniques to determine radiation dose to patients and the scanner radiation output performance. The fundamental dosimetry quantities used to describe CT dosimetry are discussed in this section.

### **2.2.1 Dose Distribution in CT**

Today, available CT scanners are generally MSCT as such dose distribution in this type of scanner is of concern, as it is an essential factor in the understanding of radiation dose that the patient receives during CT imaging. In the conventional projection radiography, dose distribution follows the Beer-lambert law of exponential decrease in applied dose (Bushberg et al., 2003). Dose decreases continuously along the y-axis from the patient part adjacent to the tube side towards its opposite side as a result of tissue attenuation of the x-ray beam as it passes through the patient's body (Figure 2.3). Consequently, a decrease in the dose is seen in the isodose line from anterior to posterior in an anterior-posterior x-ray projection of the skull, as shown in Figure 2.3. Whereas, in MSCT, the isodose line is homogeneous (Buzug, 2008). This is because the object is x-rayed from all angles and doses are accumulated across all the angles, thereby resulting in a homogeneous dose distribution inside the scanned body part.

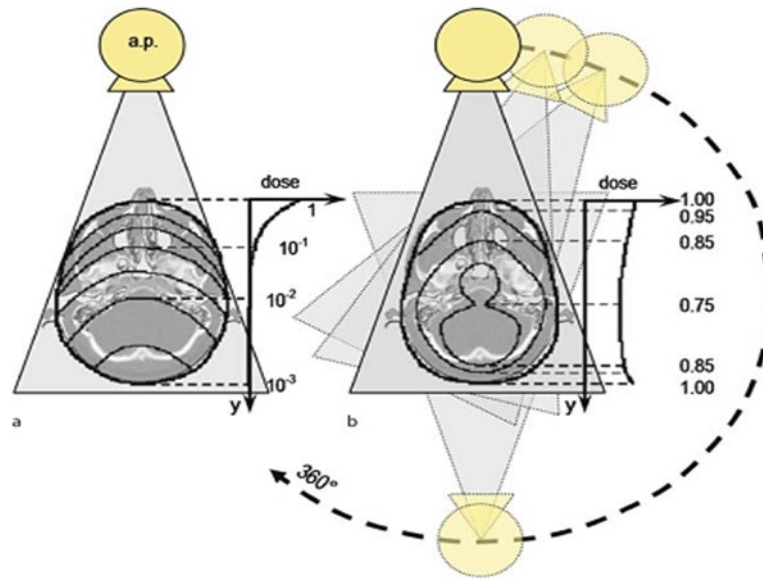


Figure 2.3 Illustration of spatial dose distribution and isodose dose lines in projection radiography (a) and CT (b). From Computed Tomography by Buzug, 2008. Copyright by Springer Nature Switzerland AG

CT image acquisition is usually limited by collimation to the desired thickness, a few millimetres. The patient is primarily irradiated in this layer. However, the measured dose profile of the reference thickness does not conform to an ideal rectangular function (Buzug, 2008). This is because the dose is given to the patient even after the reference slice or thickness adjusted by collimation; this is as a result of scatter radiation. Therefore, the dose profile in CT is specified in full-width half maximum (FWHM), and typically the nominal slice thickness lies within the FWHM (Figure 2.4). Additional doses contributed by scatter radiation outside the x-ray beam are taken care of by the computed tomography dose index (CTDI) when considering the total amount of dose in CT. CTDI is a necessary CT specific dose quantity, which conveys the total amount of dose to an ideal rectangular dose profile along the z-axis (Buzug, 2008).

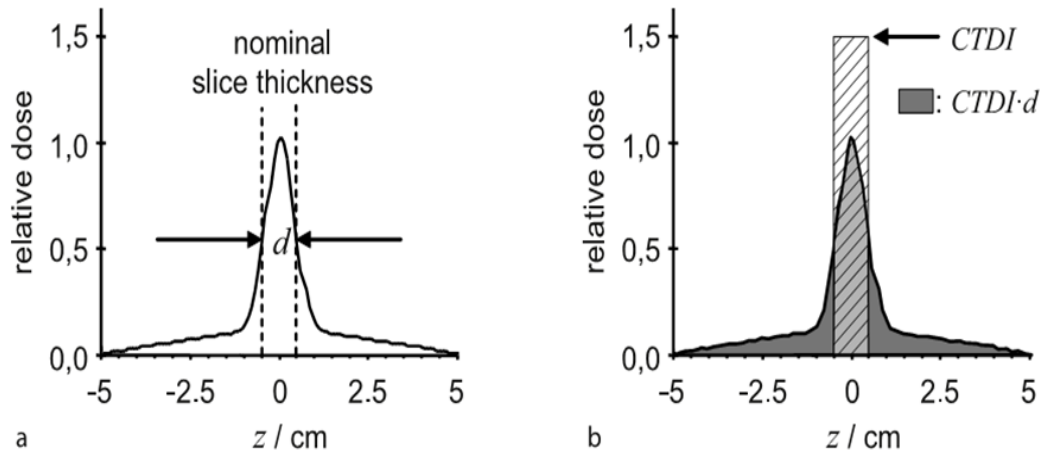


Figure 2.4 Illustration on single slice dose profile for (a) nominal slice thickness of 10mm and (b) computed tomography dose index (CTDI) obtained via the area of dose profile. ( Buzug, 2008).

### 2.2.2 CT-Specific Dose Quantities

Some CT-specific dose quantities are used for the description of the dose in CT. These dose quantities are mostly a characterisation of CT scanner radiation output that are referenced to measurements on tissue-equivalent acrylic phantoms of standard 16 cm and 32 cm diameters (Figure 2.5). The 16 cm phantom usually represents the adult head and paediatric head and body, while the 32 cm represents the adult body or torso. They include the CT dose index known as the CTDI, the "weighted" CTDI ( $CTDI_w$ ), the "volumetric" CTDI ( $CTDI_{vol}$ ) and the dose length product (DLP). The S.I units for CTDI is the mGy and DLP is measured in mGy/cm. Modern CT scanners are required by the international electrotechnical commission (IEC) to have on the scanner display at least two of these dose indices. Currently, the vast majority of scanners display the  $CTDI_{vol}$  and DLP (European Commission, 2000).



Figure 2.5 CTDI phantoms of 16 cm and 32 cm in diameter (polymethyl-Methacrylate). From CT Dose Phantoms by Universal Medical. Copyright 1983-2021 by Universal Medical

However, since the year 2011, it has been recommended that a new method of quantifying dose which modifies the  $CTDI_{vol}$  be adopted in addition to existing indices to improve the accuracy of the current CT dose index (Boone et al., 2011). This was termed the size-specific dose estimate (SSDE), and its measurement unit is the mGy.

#### Computed Tomography Dose Index (CTDI)

Computed tomography dose index (CTDI) is defined as the total amount of radiation dose to an ideal rectangular dose profile along the z-axis of the irradiated medium. The CTDI is calculated as follows:

In single-slice CT,

$$CTDI = \frac{1}{a} \int_{-\infty}^{\infty} D(z) dz \quad 2.1$$

In multi-detector CT,

$$CTDI = \frac{1}{TN} \int_{-\infty}^{\infty} D(z) dz \quad 2.2$$

Where,  $d$ = the nominal slice thickness,  $D(z)$  = radiation dose along the  $Z$ -axis,  $N$  = number of acquired tomographic sections in a single axial scan or amount of data channels used for that particular scan. The value of  $N$  may be less than equal to the maximum number of data channels available on the system (McCullough et al., 2008). And  $T$  = width of the tomographic section along the  $z$ -axis imaged by one data channel.

In multi-detector (multi-slice) CT scanners, several detector elements may be grouped to form a data channel. In a single-detector row (single slice) CT, the  $z$ -axis collimation ( $T$ ) is the nominal scan width.

#### Computed Tomography Index 100 (CTDI<sub>100</sub>)

CTDI<sub>100</sub> is a linear measure of dose distribution over a pencil ionisation chamber, it represents the accumulated multiple scan dose at the centre of a 100 mm scan and underestimates the accumulated dose for longer scan lengths. The CTDI<sub>100</sub> requires the integration of the radiation dose profile from a single axial scan over specific integration limits. The integration limits are  $\pm 50$  mm, which corresponds to the 100 mm length of the commercially available "pencil" ionisation chamber.

$$CTDI_{100} = \frac{1}{NT} \int_{-50mm}^{50mm} D(z) dz \quad 2.3$$

#### Weighted Computed Tomography Index (CTDI<sub>w</sub>)

This is the weighted average of the CTDI<sub>100</sub> measured at the centre and the periphery points in the phantom. Thus, it is closer to a human dose profile and absorbed dose average in a scan plane or single cross-section. Hence, it can be calculated from CTDI<sub>100</sub> as follows:

$$CTDI_w = \left( \frac{2}{3} CTDI_{100}(\text{periphery}) + \frac{1}{3} CTDI_{100}(\text{center}) \right) \quad 2.4$$



## Volume Computed Tomography Dose Index (CTDI<sub>vol</sub>)

The CTDI<sub>vol</sub> is a direct and easy to measure CT dose quantity, which represents the average dose within the scan volume for a standardised (CTDI) phantom. It describes a specific CT protocol which is made of a series of axial scans taking into account the gaps or overlap between x-ray beams from the consecutive rotation of the x-ray tube. These can be determined from CTDI<sub>w</sub> as follows:

$$\text{CTDI}_{\text{vol}} = \frac{N \times T}{l} \times \text{CTDI}_w \quad 2.5$$

Where  $l$  = table increment per axial in mm.

Since the pitch is defined as the ratio of table travel per rotation ( $l$ ) to the total nominal beam width ( $N \times T$ ).

$$\text{Pitch} = \frac{1}{N \times T} \quad 2.6$$

Then, CTDI<sub>vol</sub> is expressed as

$$\text{CTDI}_{\text{vol}} = \frac{1}{\text{pitch}} \times \text{CTDI}_w \quad 2.7$$

CTDI<sub>w</sub> represents the average absorbed radiation dose over the x and y directions at the centre of the scan from a series of axial scans where the scatter tails are negligible beyond the 100-mm integration limit. CTDI<sub>vol</sub> represents the average absorbed radiation dose over the x, y, and z-axis.

## Dose Length Product (DLP)

The concept DLP integrates both the dose as CTDI<sub>vol</sub> and the scanning range (Figure 2.6). It can be considered more closely related to risk. However, a significant setback of this dose index in paediatric CT dosimetry is the enormous percentage dose contributed by additional scan volume either side of the region of interest (over-

ranging) when scanning smaller patient sizes during helical scans (IAEA, 2013). Over-ranging may be critical, affecting the dose to organs at the edge of an area of interest as well as resulting to additional dose to the patient. DLP and overall dose to organs and risk are thus dependent on selected scan field of view (start and end position). CT operators are therefore encouraged to limit the anatomic area of interest to that which is only critical to patient diagnosis and benefit during CT scan as this will significantly reduce the overall risk and dose to the paediatric patient.

$$\text{DLP (mGy-cm)} = \text{CTDI}_{\text{vol}} \text{ (mGy)} \times \text{scan length (cm)} \quad 2.8$$

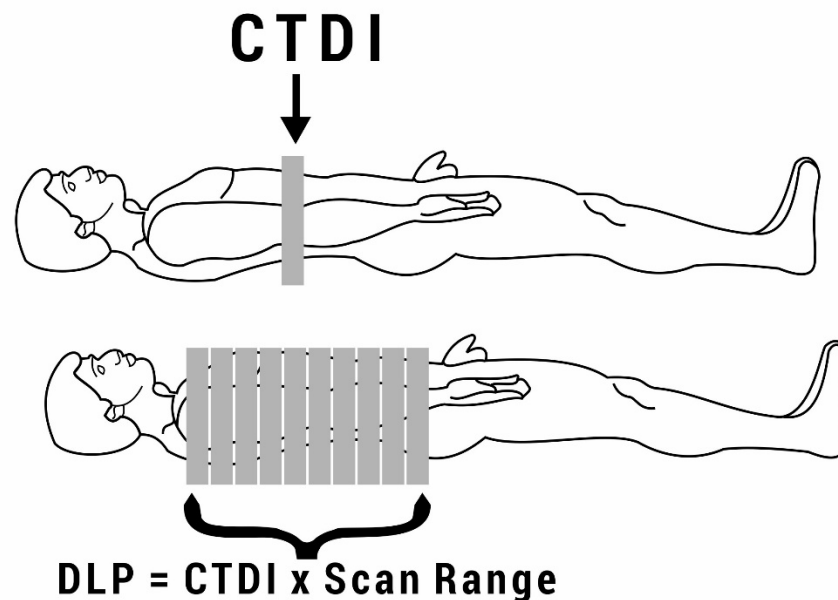


Figure 2.6 Illustration of CTDI dose quantification. From The Imaging Physicist, Radiology Physics Education. Copyright 2022

### 2.2.3 Size-specific Dose Estimate (SSDE)

SSDE is a recent CT dose estimate developed to improve the CTDI CT dose description. It is assumed to characterise the absorbed dose to patients better because the patient-specific patient size and composition are incorporated with the scanner

dose output information in this estimation (Boone et al., 2011; Brink and Morin, 2012). Size-specific dose estimation involves measuring the patient anterior (AP) and lateral (LAT) dimensions, especially in body CT (Brady and Kaufman, 2012). Initially, AAPM report 204 measurements was limited to body CT examinations and was described as measurement taken from either the axial reconstructed image or the localiser projection images at a specific reference level. However, the use of the central slice axial full field of view image along the scan volume is encouraged. More so, the relationship between attenuation and pixel values varies between CT scanners and manufacturers, thus a major reason  $D_w$  estimation using localiser image is not recommended. Using the geometric AP and LAT measurements, an effective diameter is calculated as described by the American Association of Physicist in Medicine (AAPM) Report 204 (Boone et al., 2011) as follows:

$$\text{Effective diameter, } D_{\text{eff}} = \sqrt{\text{AP} \times \text{LAT}} \quad 2.9$$

Subsequently, in 2019 an AAPM task group Report 293 introduced the use of water equivalent diameter ( $D_w$ ) as the basis of patient size determination and developed CTDI<sub>vol</sub>-to-SSDE size conversion factors for CT examinations of the head (Boone et al., 2019). The  $D_w$  accounts for patient attenuation and was coined to be more relevant in characterizing absorbed dose in comparison to the geometric based  $D_{\text{eff}}$ . It was observed that though two body parts chest and abdomen for example; could have the same geometric diameter however, differ in terms of density and composition. The chest is less dense due to presence of air in the lung fields compared to equal abdomen geometric size with more dense and tissue composition (McCollough et al., 2014).

$$\text{Water equivalent diameter, } D_w = 2 \sqrt{\left(\frac{1}{1000}HU + 1\right) \frac{A}{\pi}} \quad 2.10$$

A CTDI<sub>vol</sub>-to-SSDE size conversion factor ( $F_{\text{size}}$  16 or 32) lookup table developed by the various AAPM task group Reports are available for correction of CTDI<sub>vol</sub> dose to measured patient size (effective diameter or water equivalent diameter) depending on scanner dosimetry reference phantom sizes of either 16 or 32 cm. Correction factor corresponding to individual patient size  $D_{\text{eff}}$  or  $D_w$  calculated using equation 2.11 or 2.12 respectively is used to multiply the dose output (CTDI<sub>vol</sub>) reported for the patient. The AAPM Report 293 suggest the use of H and B as superscript as nomenclature indicating the body part for head (H) or body (B) and CTDI phantom size used for scanner dosimetry, and this described in Equation 2.11 and 2.12 (McCollough, et al., 2014).

$$\text{SSDE} = \text{CTDI}_{\text{vol},32} \times F^{\text{B32}} \quad 2.11$$

$$\text{SSDE} = \text{CTDI}_{\text{vol},16} \times F^{\text{B16}} \quad 2.12$$

Therefore, the superscript of “B32” or “B16” is used in the conversion factor ( $f$ ) when the 32 cm or 16 cm CTDI phantom size was used for the body CTDI<sub>vol</sub> measurement respectively and the 32 or 16 is added to the subscript ‘vol’ of the CTDI<sub>vol</sub> (As shown in Equation 2.13).

$$\text{SSDE} = \text{CTDI}_{\text{vol},16} \times F^{\text{H16}} \quad 2.13$$

The “B16” is to be used in the superscript of conversion factor ( $f$ ) when the 16 cm CTDI phantom size was used for the body CTDI<sub>vol</sub> measurement and a 16 is added to the subscript vol of the CTDI<sub>vol</sub>.